FEM Analysis for Comparative Investigation of The Stator Circuit Connexion Impact on The Induction Motor Broken Bar Fault Higher Order Signatures

Noura Halem[1,2], Salah Eddine Zouzou[2], Kamel Srairi[3], and Konstantinos N. Gyftakis[4]

[1]Faculty of Technology, University of El-Oued, BP 789, 39000, El-Oued, Algeria
[2]LGEB Laboratory, University of Biskra, BP 145 Biskra, Algeria
[3]LMSE Laboratory, University of Biskra, BP 145 Biskra, Algeria
[4]Dept. of Aviation, Aerospace, Electrical and Electronic Engineering, Coventry University, UK
noura.halem@yahoo.fr, zouzou_s@hotmail.com

Abstract: The induction motor operating reliability is a major issue of modern industry since faults may occur and disrupt the production process. In this work, the diagnostic potential of the line or phase current frequency spectrum for the identification of the broken bar fault in the cage induction motor is investigated depending on the stator three-phase winding configuration. The work is carried out with transient finite element method (FEM) simulations considering motor operation under nominal mechanical load. The study will concern the traditional broken bar fault signatures but also higher order harmonics and will lead to a comparison between their reliability to detect the broken bar fault, with respect to prior work.

Keywords: FEM; Induction motor; Broken bar; Fault diagnosis; Higher order signatures; MCSA

1. Introduction

In many industrial application areas, induction motors stand out because of inherent qualities such as robustness, little maintenance, low cost and simplicity. Although its advantages, induction motors are failures subjected, which are inherent to the machine itself (thermal, electrical, mechanical) or due to external environment. In this way and aiming to avoid reduced output, emergency maintenance costs, broken down equipment and lost revenues caused by faults, early fault detection and diagnosis allow preventative and condition-based maintenance.

Various techniques have been developed to detect faults in induction motor. These techniques are based on the monitoring of vibration, temperature, motor voltage, air-gap torque and current [1-3]. In the last decades, many papers have reported the effectiveness of the application of the motor current signature analysis (MCSA) for stator and rotor faults detection [4-8].

MCSA is based on the detection of new generated frequency components in stator current spectrum, or, in some cases, by the amplitudes varying of old frequency components in current spectrum. Analogically, stator current in induction motor looks as blood in human body, most diseases are detect by its analysis, in other words by appearing of new components in its content or by decreasing or increasing of existing components, in both cases a well knowledge of healthy state is strongly required. Moreover, before using MCSA, a prior knowledge of all the factors affecting on the appearance of frequency components or on its amplitudes must be available. In fact, many of the papers focused on the impact of magnetic saturation, number of rotor and stator slots upon the stator current spectrum [7-13], while a few papers deal with the impact of connection types of the feed electric circuit [14, 15].

Generally, the feed circuit of induction motor is connected using star or star delta connection. Star delta allows large motors to start with reduced starting current.

In order to keep a previously knowledge about the difference between each connection type and its influence on the amplitudes of harmonics, before heading to use signature analysis as a

Received: September 16th, 2015. Accepted: December 7th, 2016
DOI: 10.15676/ijeei.2016.8.4.3

method to diagnose induction motor default. The main problem which will be widely discussed in this paper is the effect of each connection type upon the stator current spectrum.

The most prominent harmonics in stator current spectrum are grouped as following:

- Magneto motive force (MMF) harmonics: are the most prominent harmonics in stator current spectrum of induction motor, their occurrence is in accordance with the definition of MMF, a result of current flowing through the corresponding winding and a consequence of the discrete nature of the stator windings.
- Saturation harmonics: due of the main flux path.
- Rotor slot harmonics (RSH): their existence is not only dependent on the MMF, stator and rotor presence and the notching nature of stator and rotor, but they also exist in the stator current spectrum only for a combined number of stator slots, rotor bars and pole pairs.

One of difficult issues in induction motor modeling is the conserving the discrete nature of stator and rotor as well as the non-linearity behavior of ferromagnetic material. The time stepping finite element method (TSFEM) avoids these difficulties by its conserving of the real geometry and electromagnetic behavior of motor.

In this paper, the FEM model of induction motor is simulated for two types of stator electric circuit connection; star connection with considering variation of neutral point potential and delta-connection. Then, the FFT (Fast Fourier Transform) is applied on extracted currents waveforms of the three simulations for healthy and faulty motors in order to show the impact of each connection on the spectrum content and detect differences between three cases.

The objective of this paper is to make a clear characterization of the stator winding configuration impact on the identification of the broken bar fault in the cage induction motor around the fundamental as well as the higher order signatures.

The paper consists of four sections as follows: section 1 is introduction; section 2 presents the harmonic index of the component of the air gap magnetic flux density with analytical calculations and a short overview on the modeling of induction motor using TSFEM, while section 3 summarizes the simulation results and interpretations. Finally, a conclusion summarizes this work's findings.

2. Theory

A. Analytical calculation

A.1. Stator and rotor MMF

For an induction motor with p pole pairs, besides the fundamental harmonic, the symmetrical three-phase stator winding produces a series of MMF terms, which are given by the well-known relation [10, 11]:

$$F_s = \sum_{m=6g\pm1}^{\infty} F_{\kappa m} \cos\left(m p\theta_s \mp \omega t\right) \tag{1}$$

Where m is the harmonic order, which is given by:

$$m = 6g + 1, \qquad g = 0, \pm1, \pm2, \ldots \tag{2}$$

The reaction of the rotor cage on the flux density waves from stator is given by the following MMF waves [11, 16]:

$$F_r = \sum_{\mu=1}^{\infty} F_{r\kappa} \cos\left(s_m \omega t \pm \left((\lambda R/p) \mp m\right) p\theta_r\right) \tag{3}$$

$$\mu = g(R/p) \pm 1 \tag{4}$$

s_m is slip of MMF m^{th} order harmonic:

$$s_m = 1 - m(1-s) \tag{5}$$

A.2. Slot permeance harmonics

The slot permeance variation due to stator and rotor slots plays a big role in the RSH generation. It can be given by [10, 11]:

$$P(\theta_s, \theta_r) = 1/g_0 + P_s \cos(S\theta_s) + P_r \cos(R\theta_r) + P_{sr} \cos(S\theta_s - R\theta_r) + \ldots \tag{6}$$

The coefficients P_s, P_r and P_{sr} are related to the stator and rotor slot geometrical variables. Considering that the stator MMF waves are given at the following position:

$$F_{sm}(t, \theta_s) = F_{s\kappa \max} \cos(\omega t - m p \theta_s) \tag{7}$$

By interacting with (7), the following components are resulted in the stator referenced flux density:

$$F_1 = B_{sm\max} \cos\left[\left(1 \mp (R/p)(1-s)\right)\omega t \pm \left(R/p \mp m\right) p\theta_s\right] \tag{8}$$

$$F_2 = B_{sm\max} \cos\left[\left(1 \mp (R/p)(1-s)\right)\omega t \mp \left((S-R)/p\right) \pm m\right) p\theta_s\right] \tag{9}$$

2.1.3. Saturation harmonics

According to [16], the air-gap relative permeance takes the following form in order to take into account the iron core saturation, considering the fundamental harmonic:

$$P(\theta_s) \approx P_0 + P_{sat}(\theta_s, t) \tag{10}$$

Where:

$$P_{sat}(\theta_s, t) = -P_{sat} \cos(2p\theta_s - 2\omega_1 t - 2\varphi_s) \tag{11}$$

The influence of the rotor and stator MMF on the magnetic flux density due to the saturation is given by [16]:

$$b_{sat}(\theta_s, t) = \left[F_s(\theta_s, t) + F_r(\theta_s, t)\right] P_{sat}(\theta_s, t) \tag{12}$$

$$b_{sat}(\theta_s, t) = -P_{sat}\, 1/2 \left[\begin{array}{l} \displaystyle\sum_{m=6g\pm1}^{\infty} F_{m\kappa} \left\{ \begin{array}{l} \cos\left[(m+2)p\theta_s - (2\omega_1 \pm \omega)t - 2\varphi_s\right] \\ +\cos\left[(m-2)p\theta_s + (2\omega_1 \mp \omega)t + 2\varphi_s\right] \end{array} \right\} \\ \displaystyle+\sum_{\mu=1}^{\infty} F_{m\mu} \left\{ \begin{array}{l} \cos\left[(\mu+2)p\theta_s - (2\omega_1 \pm \omega)t - (\varphi + 2\varphi_s)\right] \\ +\cos\left[(\mu-2)p\theta_s + (2\omega_1 \mp \omega)t - (\varphi - 2\varphi_s)\right] \end{array} \right\} \end{array} \right] \tag{13}$$

B. Induction motor modeling using TSFEM

In this paper, the TSFEM is used for modeling and analyzing of healthy and faulty motor using circuit-coupled method. The transient equations of the external electric circuit presenting the three-phase sinusoidal voltage is coupled with the field equations in FEM of magnetic circuit which containing the geometrical and physical characteristic of motor such as non-linear characteristic of lamination core. Also, the motion equations are combined with the field [17]. Figure 1 presents the cross-sectional geometry of the motor, whereas Table 1 illustrates the characteristics of the motor used.

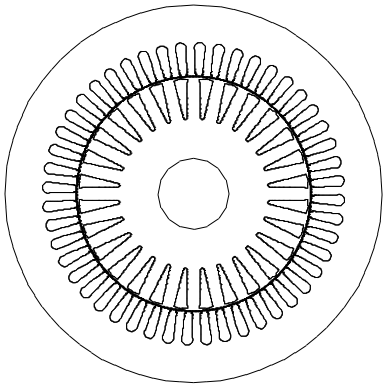

Figure 1. Cross-sectional geometry of the 1.1 kW cage induction motor.

Table 1. Specifications of simulated induction motor.

Number of poles	4
Number of phases	3
Rated power (kW)	1.1
Rated voltage (V)	230
Frequency (Hz)	50
Rated speed (rpm)	1425
Number of stator slots	48
Number of rotor slots	28

The input values are the three phase sinusoidal voltages, while the principle and required variable is the stator current. The field equations in FEM are coupled with the transient equations of the external circuit showing the electric supplies and circuit elements with. The motion equations are combined with the field equations in the FEM. Two-dimensional magnetic field propagation is given by:

$$\vec{\nabla} \times \nu \vec{\nabla} \times \vec{A} = \vec{J}_0 \tag{14}$$

Where ν is the magnetic reluctivity, $\vec{A}$ is the magnetic potential vector and $\vec{J}_0$ is the current density in the z-axis direction.

According to equation (14), the total current of each conductor is obtained by integration of (14) over the cross section of the conductor as follows:

$$J_0 = \delta \partial A/\partial t - \delta \Delta \upsilon / l \tag{15}$$

Where δ is the electrical conductivity, *t* is the time, $\Delta \upsilon$ is the potential difference along the length of the conductor and *l* is the conductor length.
From (14) and (15):

$$\nabla \times \nu \nabla \times A = \delta \partial A/\partial t - \partial \Delta \upsilon / l \tag{16}$$

In order to link the field and circuit equations, it is necessary to estimate the total current of every conductor. Therefore, by integrating J_0 over the cross-sectional area, the current will be as follows:

$$i = \iint \delta \left(\partial A/\partial t - \Delta \upsilon / l \right) ds \tag{17}$$

This current passes through the supply, resistance R_{ext} and inductance L_{ext}. Therefore:

$$V_s = R_{ext}\, i + L_{ext}\, di/dt + E \tag{18}$$

Where E is the induced voltage in the finite element region, *Vs* is the applied voltage. The following general equation is [18, 19]:

$$\left[P\right]\left[A \quad E \quad i\right] + \partial/\partial t\left(\left[A \quad E \quad i\right]^T\right) = \begin{bmatrix} J_0 \\ 0 \\ -V_s \end{bmatrix} \tag{19}$$

The magnetic potential distribution and stator phase current required for applying the Fast Fourier Transform (FFT) are obtained by solving (19).

3. Simulations results

A. The case of Y connection

In this case the stator windings form a Y connection as it can be seen in Figure 2.

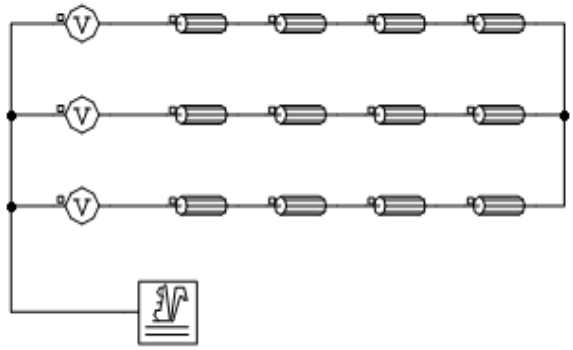

Figure 2. The stator windings in Y connection

The frequency spectrums of the line current for healthy and faulty operation are presented in Figure 3. In Figure 3a, the vertical arrows point the rotor slot related harmonics, whereas the horizontal ones the MMF related harmonics (50Hz, 250Hz, ...) and the saturation related

harmonic at 150Hz. In figure 3b, the broken bar related harmonics can be observed, located at frequencies $(n \pm 2ks) f_s$. For a better overview of the fault's signatures amplitudes, Table 2 summarizes the different broken bar fault signatures amplitudes compared to the healthy motor.

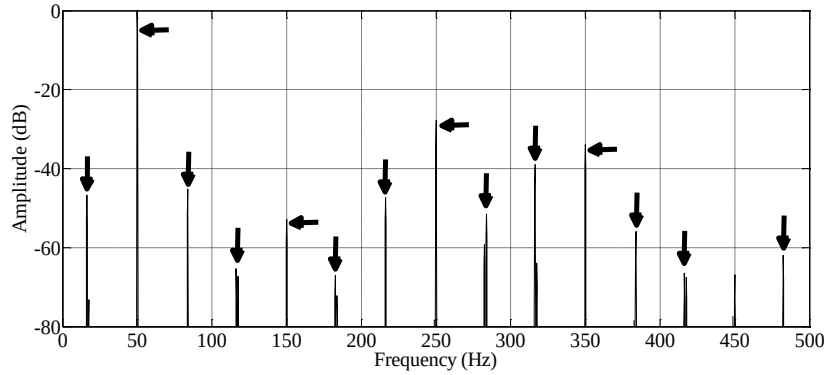

(a)

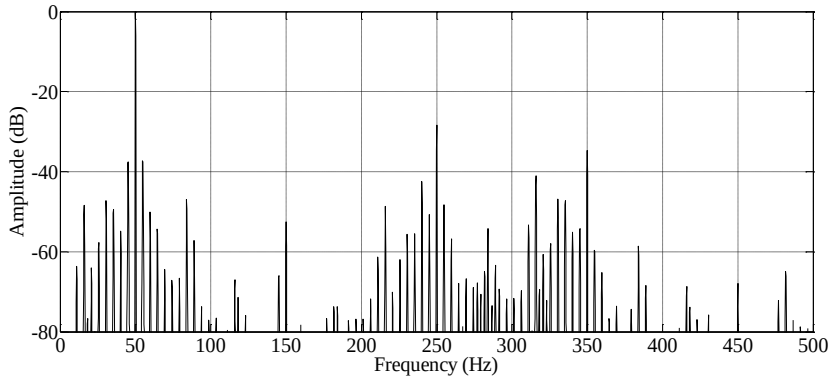

(b)

Figure 3. The line current frequency spectrums for Y connection. healthy motor, (b) motor with a broken bar.

Table 2. Broken bar fault signatures amplitudes in Y connected healthy and faulty motors current spectrum.

	Healthy	Faulty
Frequency (Hz)	Amplitude (dB)	
45.25	-91.93	-37.53
54.75	-83.12	-37.27
145.3	-106.3	-65.96
240.3	-87.63	-42.43
245.3	-85.37	-50.74
254.8	-84.69	-48.26
259.8	-100.6	-56.75
330.5	-94.1	-46.9
335.5	-100.6	-47.28
340.3	-105.6	-55.1
345.3	-86.69	-54.15
355	-102.7	-59.93
359.8	-103	-65.15

From Table 2, it is clear that for this specific applied load, best fault signatures are the traditional sideband to 50Hz harmonics (at 45.25Hz and 54.75Hz), since they present the greatest amplitudes. The signature close to the third current harmonic at 145.3Hz clearly indicates the fault's existence but its amplitude is not very strong (-65.96dB). On the other hand, the signatures close to the fifth and seventh current harmonics are characterized by important amplitudes, also revealing the broken bar fault. For all signatures, it is clear that they have about 35-50dB greater amplitudes than those of the healthy motor.

B. The case of Y-N connection

In this case the stator winding forms a Y connection with neutral. The electric circuit can be seen in Figure 4.

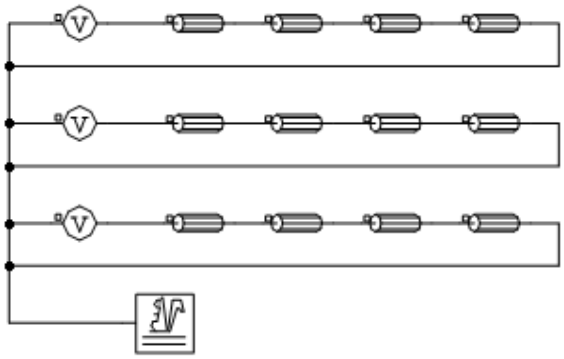

Figure 4. The stator winding in Y-N connection.

The frequency spectrums of the line current for healthy and faulty operation are presented in Figure 4. In Figure 4a, the vertical arrows point the rotor slot related harmonics, whereas the horizontal ones the MMF related harmonics (50Hz, 250Hz, ...) and the saturation related harmonic at 150Hz. In figure 4b, the broken bar related harmonics can be observed, located at frequencies $\left(n \pm 2ks\right) f_s$. Table 3 presents the different broken bar fault signatures amplitudes compared to the healthy motor.

Table 3. Broken bar fault signatures amplitudes in Y-N connected healthy and faulty motors current spectrum.

	Healthy	Faulty
Frequency (Hz)	Amplitude (dB)	
45	-91.71	-37.17
55	-84.39	-36.55
140.3	-76.13	-31.18
145	-85	-33.83
155	-79.22	-42.78
240.3	-83.06	-39.07
245	-83.24	-47.12
255	-93.76	-51.51
330.5	-93.92	-46.17
335.3	-99.65	-46.75
340.3	-94.8	-53.69
345.3	-95.14	-50.09
355	-90.87	-58.27

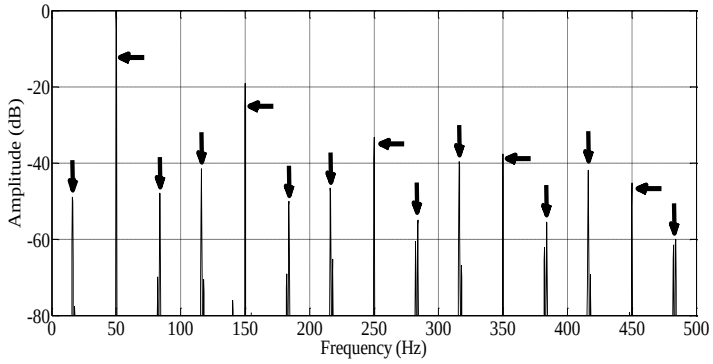

(a)

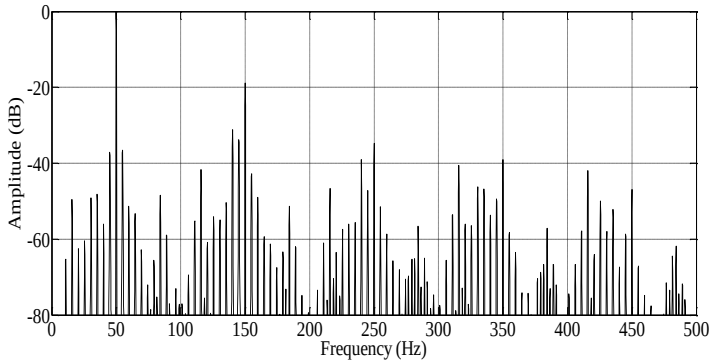

(b)

Figure 5. The line current frequency spectrums for Y-N connection. (a) healthy motor, (b) motor with a broken bar.

C. The case of Δ connection

The delta connection offers two different possible current waveforms for the broken bar fault diagnosis: the line and the phase current. Usually, in already existing installations the line current is the most practical to measure. Nevertheless, both currents have been used in the past. In this paper, both the two spectrums for phase and line currents will be investigated. In figure 5, the electrical circuit used for the delta connection is presented.

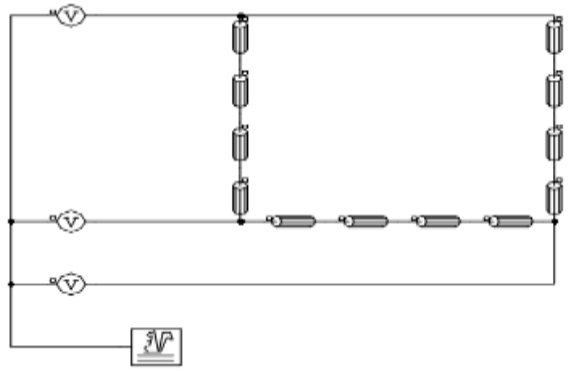

Figure 6. The stator windings forming a delta connection

The frequency spectrums of the line current for healthy and faulty operation are presented in Figure 7, where as in Figure 8, the phase current spectrum for the healthy motor and the one

with the broken bar are also illustrated. In figure 7a and figure 8a, the vertical arrows point the rotor slot related harmonics, whereas the horizontal ones the MMF related harmonics (50Hz, 250Hz, ...) and the saturation related harmonic at 150Hz. In figure 7b and figure 8b, the broken bar fault related harmonics can be observed, located at frequencies $\left(n \pm 2ks\right) f_s$.

Tables 4 and 5 present the different broken bar fault signatures amplitudes compared to the healthy motor for the line and phase current respectively.

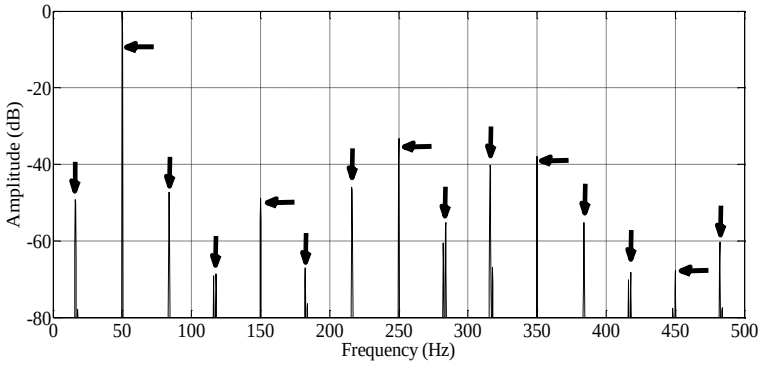

(a)

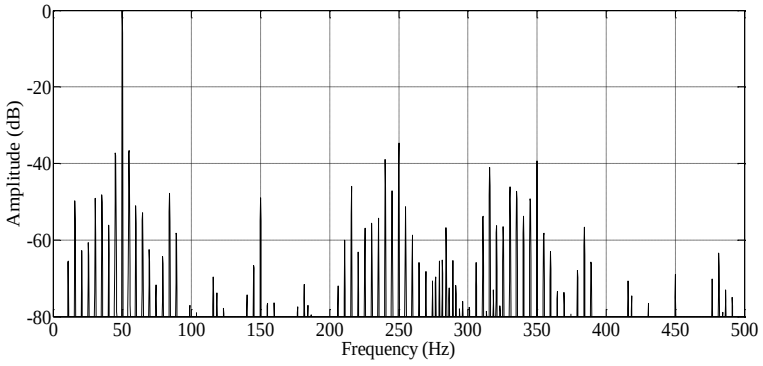

(b)

Figure 7. The line current frequency spectrums for Δ connection. (a) health, (b) faulty motors.

Table 4. Broken bar fault signatures amplitudes in Y-N connected healthy and faulty motors line current spectrum.

	Healthy	Faulty
Frequency (Hz)	Amplitude (dB)	
45	-93.58	-37.24
55	-83.71	-36.6
145	-111.6	-66.69
240.3	-83.18	-38.97
245	-83.33	-47.21
255	-92.65	-51.35
330.5	-94.18	-46.12
335.3	-100.5	-47.26
340.3	-95.12	-53.73
345	-93.44	-49.18
355	-90.36	-58.19

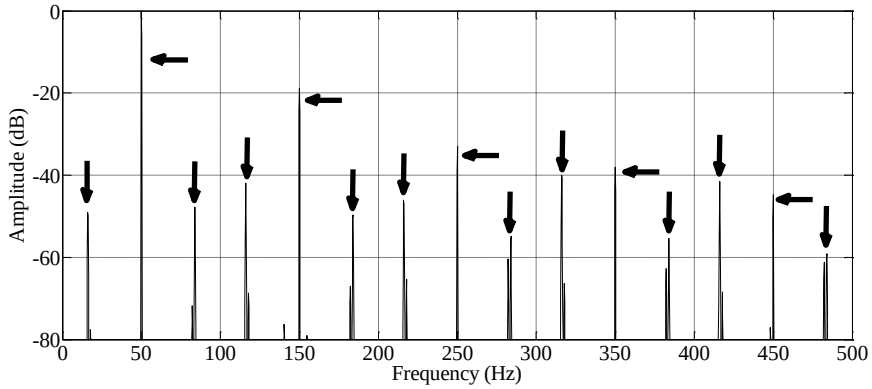

(a)

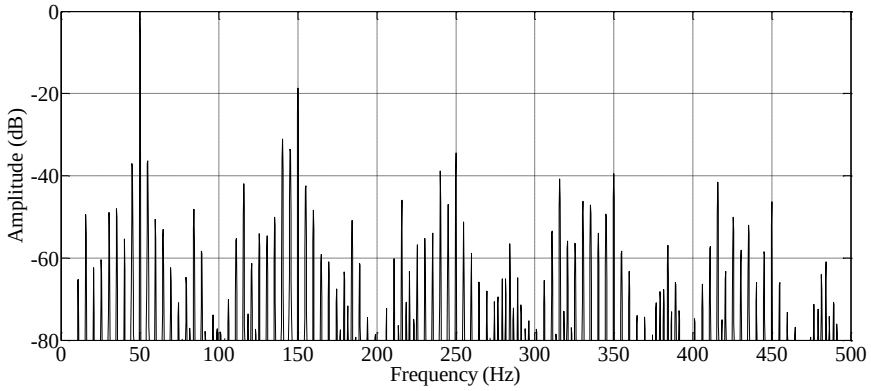

(b)

Figure 8. The phase current frequency spectrums for Δ connection.
(a) healthy, (b) faulty motors.

Table 5. Broken bar fault signatures amplitudes in Y-N connected healthy and faulty motors phase current spectrum.

	Healthy	Faulty
Frequency (Hz)	Amplitude (dB)	
45	-92.16	-37.64
55	-84.69	-36.42
140.3	-76.25	-31.13
145.3	-85.38	-34.25
155	-78.97	-42.46
240.3	-82.85	-38.87
245	-83.16	-46.96
255	-93.55	-51.28
330.5	-94.26	-46.14
335.3	-100.6	-47.12
345	-93.73	-49.3

D. Discussion of the simulation results

In this section, the simulation results will be thoroughly investigated and discussed with respect to prior work. Traditional MCSA method requires to detect the broken bar fault close to the base current harmonic (50Hz) at frequencies $\left(1\pm 2ks\right) f_s$. Moreover, other works propose the detection of the broken bar fault close to the third current harmonic, which is also saturation related, at frequencies $\left(3\pm 2ks\right) f_s$ [20, 21]. Furthermore, it has also been proposed to monitor the sideband signatures close to the fifth and seventh current harmonics [20, 22].

Generally, at high and nominal load, the traditional signatures close to the current base harmonic are reliable. The above harmonics become unreliable at low load operation [23] and also they get weak when the saturation level of the induction motor is high [24]. So, it was shown in [25], that higher order signatures are more reliable when it comes to the broken bar fault detection at low load condition. Keeping all this in mind, several remarks can be obtained through this work's simulation results and the comparative investigation depending on the stator winding's connection type.

Firstly, it can be seen through Tables 2, 3, 4 and 5 that the broken bar fault signatures close to the 50Hz current harmonic have similar and reliably high amplitudes compared to the healthy cases. This result was expected since the motor operated under nominal load and the slip is not very low, adjacent to 2.5%.

Secondly, it is worth mentioning that the broken bar fault can be reliably identified close to the saturation related 150Hz current harmonic in two of the four studied cases: in the line current frequency spectrum of the Y-N connection (Table 3) and the phase current frequency spectrum of the Δ connection (Table 5). It is important to mention that, the signatures at 140Hz and 145Hz for the above cases present even greater amplitudes (2-6dB) than the traditional signatures close to the base current harmonic. Also, the harmonic at 140Hz is less sensitive to the slip level of the motor's operation. So, here lies an advantage over the traditional MCSA method's signatures. In the other two cases (Tables 2 and Table 4), the broken bar fault signatures close to the 150Hz harmonic do not present important amplitudes compared to other signatures of the spectrum. But it is worth saying that the third line current harmonic is sensitive to the grid's voltage imbalance [26]. So, in real operating conditions if a voltage supply asymmetry exists, then the signatures of the line currents, for Y and Δ connection, close to the 150Hz current harmonic would present greater amplitudes as well. But, under symmetrical three phase voltage, they are unreliable. Furthermore, the broken bar fault signature at 240.3Hz close to the fifth current harmonic, presents increased amplitude comparative to the traditional signatures. Especially for the Δ connection (Tables 4 and Table 5), this specific harmonic is characterized by similar amplitude to the traditional ones close to the base harmonic (about 1dB amplitude difference). Practically speaking, this is an advantage since the 240.3Hz harmonic rests close to the 250Hz MMF related harmonic which has much less amplitude compared to the basic one, thus making the diagnosis easier and more reliable.
Finally, the harmonics at 330.5Hz and 335.5Hz are characterized in all cases by similar amplitudes (about -47dB). Although in this paper's studied cases, this amplitude is lower than the traditional signatures, one should think that at low load condition those harmonics are much less slip sensitive and can reliably reveal the broken bar fault as it was shown in [25].

4. Conclusion

This paper studied the impact of the stator winding configuration on the phase and line current frequency spectrum of the cage induction motor aiming to the diagnostic ability of the broken bar fault. The results show that the broken bar fault signatures close to the third current harmonic are stronger than the traditional ones for the case of the Y-N connection and the phase current of Δ connection. Moreover, the signatures close to the fifth current harmonic offer similar diagnostic potential to the traditional ones for all cases and at the same time they seem to be less slip sensitive. So, they could be more reliable while the applied mechanical

load decreases. Furthermore, in the case of Y connection the traditional signatures seem to be the most prominent choice if the motor operated under nominal load.

Finally, the broken bar fault signatures close to the seventh current harmonic are about 10dB less than the traditional ones for all studied cases, but, they seem the least slip sensitive and they could be also used for low load operation for the reliable broken bar fault detection. Future work should concern the investigation of the current spectrum for different stator winding connections for different load and saturation levels as well as experimental testing.

Nomenclature

f_s : Stator frequency

p : Number of pole pairs

S : Stator slot number

R : Rotor slot number

n_d : Eccentricity order

g : Ordinal number

λ : Harmonic order

g_0 : Air-gap length

t : Time

ω : Angular frequency

s : Slip

s_m : Slip of MMF m^{th} order harmonic

$F_{s\kappa}$: Stator MMF amplitude

$F_{1\kappa}$, $F_{2\kappa}$, $F_{3\kappa}$: Stator MMF amplitudes

P_{sat} : Air-pap relative permeance saturation component

φ, φ_1, φ_s : Phase angles

5. Acknowledgement

The authors would like to thank Professor Champenois from the LAII laboratory, Poitiers, France, for his help.

6. References

[1]. C. Concari, G. Franceschini, C. Tassoni, "Differential diagnosis based on multivariable monitoring to assess induction machine rotor conditions", *IEEE Transaction on Industrial Electronics, vol. 55 no. 12, pp. 4156-4166, 2008*.

[2]. K. N. Gyftakis, D. V. Spyropoulos, J. C. Kappatou and E. D. Mitronikas, "A novel approach for broken bar fault diagnosis in induction motors through torque monitoring", *IEEE Trans. Energy Conversion, vol. 28, no. 2, pp. 267-276, 2013*.

[3]. M.J. Picazo-Ródenas, R. Royo, J. Antonino-Daviu, J. Roger-Folch, "Use of the infrared data for heating curve computation in induction motors: Application to fault diagnosis", *Engineering Failure Analysis, vol. 35, pp. 178-192, 2013*.

[4]. W. T. Thomson and A. Barbour, "On-line current monitoring and application of finite element method to predict the level of static airgap eccentricity in three-phase induction motors", *IEEE Trans. Energy Conversion, vol. 13, no. 4, pp. 347-357, 1998*.

[5]. N. Halem, K. Srairi, S. E. Zouzou, "Stator Current Signature Analysis of Healthy Motor Using Time Stepping Finite Element Method", *International Journal on Electrical Engineering and Informatics, vol. 6, no. 1, pp. 144-154, 2014*.

[6]. M. Sahraoui, A. Ghoggal, S. E. Zouzou, M.E. Benbouzid, "Dynamic eccentricity in squirrel cage induction motors –simulation and analytical study of its spectral signatures on stator currents", *Simulation Modelling Practice and Theory, vol. 16, no. 4, pp. 1503-1513, 2008*.
[7]. K. N. Gyftakis, and J. C. Kappatou, "A novel and effective method of static eccentricity diagnosis in three-phase PSH induction motors", *IEEE Trans. Energy Conversion, vol. 28, no. 2, pp. 405-412, 2013*.
[8]. N. Feki, G. Clerc, and Ph. Velex, "Gear and motor fault modeling and detection based on motor current analysis", *Electric Power Systems Research, vol. 95, pp. 28-37, 2013*.
[9]. S. Nandi, "A detailed model of induction machines with saturation extendable for fault analysis", *IEEE Trans. Industry Application, vol. 40, no. 5, pp. 1302-1309, 2004*.
[10]. S. Nandi, "Modeling of induction machines including stator and rotor slot effects", *IEEE Trans. Industry Application, vol. 40, no. 4, pp. 1058-1065, 2004*.
[11]. G. M. Joksimovic, J. Riger, T. M. Wolbank, N. Peric, and M. Vasak, "Stator-current spectrum signature of healthy cage rotor induction machines", *IEEE Trans. Industrial Electronics, vol. 60, no. 9, pp. 4025-4033, 2013*.
[12]. G. Joksimovic, "Line current spectrum analysis in saturated three-phase cage induction machine. Electrical Engineering", *Springer. Verlag, vol. 91, no. 8, pp.425-437, 2010*.
[13]. N. Halem, S. E. Zouzou, K. Srairi, S. Guedidi and F. Abood, "Static eccentricity fault diagnosis using the signatures analysis of stator current and air gap magnetic flux by finite element method in saturated induction motors", *Int. J. Syst. Assur. Eng. Manag, vol. 4, no. 2, pp. 118-128, 2013*.
[14]. P. Pillay, R. G. Harley and E. J. Odendal, "A comparison between star and delta connected induction motors when supplied by current sources inverters", *Electric Power Systems Research, vol. 8, pp. 41-51, 1984/85*.
[15]. K. Yamazaki and S. Shinfuku, "Combined 3-D–2-D finite element analysis of induction motors considering variation of neutral point potential in star connection", *IEEE Trans. Magnetics, vol. 37, no. 5, pp. 3706-3710, 2001*.
[16]. K. N. Gyftakis and J. Kappatou, "The impact of the rotor slot number on the behavior of the induction motor", *Advances in Power Electronics, pp. 1-9, 2013*.
[17]. A. B. J. Reece and T.W. Preston, "Finite element methods in electrical power engineering", *Oxford Science Publication, 2000*.
[18]. J. Faiz, B. M. Ebrahimi, B. Akin, and H. A. Toliyat. "Dynamic analysis of mixed eccentricity signatures at various operating points and scrutiny of related indices for induction motor", *Electric Power Applications, vol. 4, no. 1, pp. 1-16, 2010*.
[19]. B. M. Ebrahimi, J. Faiz, S. Lotfi-fard and P. Pillay. "Novel indices for broken rotor bars fault diagnosis in induction motors using wavelet transform", *Mechanical Systems and Signal Processing, vol. 30, pp. 131-145, 2012*.
[20]. H. Henao, H. Razik and G. A. Capolino, "Analytical approach of the stator current frequency harmonics computation for detection of induction machine rotor faults", *IEEE Trans. Industry Application, vol. 41, no. 3, pp. 801-807, 2005*.
[21]. A. Khezzar, M. Y. Kaikaa, M. E. K. Oumaamar, M. Boucherma and H. Razik, "On the use of slot harmonics as a potential indicator of rotor bar breakage in the induction machine", *IEEE Trans. Industrial Electronics, vol. 56, no. 11, pp. 4592-4605, 2009*.
[22]. J. Cusido, J. Rosero and E. Aldabas, "New fault detection techniques for induction motors", *Electrical Power Quality and Utilisation. Magazine 2, no. 1, 2006*.
[23]. J. Sprooten and J. C. Maun, "Influence of saturation level on the effect of broken bars in induction motors using fundamental electromagnetic laws and finite element simulations", *IEEE Trans. Energy Conversion, vol. 24, no. 3, pp. 557-564, 2009*.
[24]. R. Puche-Panadero, M. Pineda-Sanchez, M. Riera-Guasp, J. Roger-Folch, E. Hurtado-Perez and J. Perez-Cruz, "Improved resolution of the MCSA method via Hilbert transform, enabling the diagnosis of rotor asymmetries at very low slip", *IEEE Trans. Energy Conversion, vol. 24 no. 1, pp. 52-59, 2009*.

[25]. K. N. Gyftakis, D. K. Athanasopoulos and J. Kappatou, "Evaluation of different broken bar fault diagnostic means in double-cage induction motors with FEM", *9th IEEE International Symposium on Diagnostics for Electric Machines, Power Electronics and Drives (SDEMPED), 27-30 August 2013,* Valencia, *Spain, pp. 36-42, 2013*.

[26]. K. N. Gyftakis, D. K. Athanasopoulos and J. Kappatou, "Broken bar fault diagnosis in single and double cage induction motors fed by asymmetrical voltage supply", *9th IEEE International Symposium on Diagnostics for Electric Machines, Power Electronics and Drives (SDEMPED), 27-30 August 2013,* Valencia, *Spain, pp. 402-406, 2013*.

Noura Halem received the *B.Sc*. degree in electrical engineering from the University of Biskra, Algeria, in 2007, and the *M.Sc*. degree in electrical networks from the Science and Technology Institute of El-Oued University Center, Algeria, in 2010. She is received the doctor of science degrees from the university of Biskra, Algeria in 2015. She is interested in the modeling, conception, and faults diagnosis of electrical machines.

Salah Eddine Zouzou was born in Biskra, (Algeria) in 1963. He received the B.S degree from the "Ecole Nationale Polytechnique d'Alger", Algeria in 1987 and the M.S and Ph.D degrees from the "École Nationale Polytechnique de Grenoble" France, in 1988 and 1991 respectively. His fields of research interests deal with the design and condition monitoring of electrical machines. He has authored or co-authored more than 50 scientific papers in national and international conferences and journals. Prof. Zouzou is a Professor at the University of Biskra, Algeria and he is the director of the "Laboratoire de Génie Electrique de Biskra" since 2003.

Kamel Srairi was born in Batna, Algeria, in 1967. He received the *B.Sc.* degree in Electrical Engineering, in 1991, from the University of Batna, Algeria; the *M.Sc.* degree in Electrical and Computer Engineering, from the National Polytechnic Institute of Grenoble, France, in 1992; and the *Ph.D.* degree also in Electrical and Computer Engineering, from the University of Nantes, France, in 1996. After graduation, he joined the University of Biskra, Algeria, where he is a Professor in the Electrical Engineering Department His main research interests include analysis, design, optimization and control of electric systems.

Konstantinos N. Gyftakis was born in Patras, Greece, in May 1984. He received the diploma in Electrical and Computer Engineering from the University of Patras, Patras, Greece in 2010. He fulfilled his obligations as a Ph.D Candidate in the Department of Electrical and Computer Engineering, University of Patras. Afterwards, he was employed as a Post Doctoral Research Assistant in the Dept. of Engineering Science, University of Oxford, UK (Nov. 2014-Sep. 2015) where he worked on degradation of electric motors for electric vehicles. He is currently a Lecturer in the Dept. of Aviation, Aerospace, Electrical and Electronic Engineering, Coventry University, UK. His research interests are in fault diagnosis and degradation of electrical machines. He has authored/co-authored more than 25 papers in international scientific journals and conferences. He is an IEEE member, member of IEEE PES, IAS, IES and Magnetics Society, member of the HELIEV (Hellenic Institute of Electric Vehicles) and finally member of the Technical Chamber of Greece. (E-mail: k.n.gyftakis@ieee.org).